Characterization of the bottlenecks and pathways for inhibitor dissociation from [NiFe] hydrogenase

Farzin Sohraby, Ariane Nunes-Alves*

Institute of Chemistry, Technische Universität Berlin, Straße des 17. Juni 135, 10623 Berlin, Germany
*Corresponding author: ferreira.nunes.alves@tu-berlin.de

Abstract

[NiFe] hydrogenases can act as efficient catalysts for hydrogen oxidation and biofuel production. However, some [NiFe] hydrogenases are inhibited by gas molecules present in the environment, such as O_2 and CO. One strategy to engineer [NiFe] hydrogenases to achieve O_2 and CO-tolerant enzymes is by introducing point mutations to block the access of inhibitors to the catalytic site. In this work, we characterized the unbinding pathways of CO in complex with the wild type and 10 different mutants of [NiFe] hydrogenase from *Desulfovibrio fructosovorans* using τ-Random Accelerated Molecular Dynamics (τRAMD) to enhance the sampling of unbinding events. The residence times computed with τRAMD are in agreement with the experimental ones. Extensive data analysis of the simulations revealed that, from the two bottlenecks proposed in previous studies for the transit of gas molecules (residues 74 and 122, and residues 74 and 476), only one of them (residues 74 and 122) effectively modulates diffusion and residence times for CO. We also computed pathway probabilities for the unbinding of different gas molecules from the wild type [NiFe] hydrogenase and we observed that, while the most probable pathways are the same, the secondary pathways are different. We propose that mutations to block the most probable paths, in combination with mutations to open the main secondary path used by H_2, can be a feasible strategy to achieve CO and O_2 resistance in the [NiFe] hydrogenase from *Desulfovibrio fructosovorans.*

Keywords: [NiFe] hydrogenase, molecular dynamics simulations, kinetic rates, residence times, unbinding pathways.

Introduction

The hydrogenase family of enzymes are key for H_2 transformation in many microorganisms and they have recently attracted attention due to their ability to act as efficient catalysts to oxidize hydrogen and produce biofuel ($H_2 \rightleftharpoons 2\ H^+ + 2\ e^-$) or even act as part of light-driven production pipelines of H_2 through water splitting[1–6]. However, some of the members of this family of enzymes are inhibited or irreversibly damaged and destroyed by gas molecules present in the environment, such as O_2 and CO[7–10]. Therefore, efforts have been made to develop strategies to rectify this problem and achieve tolerant enzymes[11–21]. One possible strategy to achieve tolerant enzymes can be blocking the access of these inhibitors to the catalytic site by designing mutant forms through tunnel engineering[16,22–28]. The difference in size and dipole moment between the substrate and the inhibitor molecules of the hydrogenases suggests that this strategy is feasible. Tunnel engineering can be used to change the preferences of an enzyme for binding to and accommodating specific ligands by site-specific point mutations[23,25,29,30]. In hydrogenases, the active site is buried in the core of the enzyme and ligands need to travel a long distance through the tunnels to reach it. In 2005, Buhrke et al.[31] reported that an oxygen-tolerant hydrogenase from *Ralstonia eutropha H16* can become sensitive to O_2 by introducing specific point mutations which expand the tunnels leading to the active site, which ultimately facilitate the access of O_2. This is evidence that tunnel engineering is a feasible strategy to achieve CO and O_2 tolerant hydrogenases[31].

Leroux et al. introduced protein film voltammetry, an experimental method that enabled the study of kinetics of binding and release of CO and other gas molecules from [NiFe] hydrogenases in a quantitative manner[28]. Using this technique, they quantified the diffusion of CO, H_2 and O_2 inside the [NiFe] hydrogenase from *Desulfovibrio fructosovorans* (Figure 1A)[32]. In the work of Liebgott et al., point mutations in this [NiFe] hydrogenase were introduced with the goal of understanding how changes in the structure of the tunnels can modulate the diffusion of gas molecules[14,32]. They created 10 different mutants, with mutations at positions V74 and/or L122 of the large subunit (Figure 1B). Such residues were chosen because inspection of the crystal structure led to the hypotheses that the distance between these two residues was the main bottleneck for gas diffusion[28,32]. Indeed, they observed changes in the kinetic rates of the

inhibitors for binding and unbinding by orders of magnitude[32]. Although the mutants delayed the binding of the inhibitors to the catalytic site, none of the mutants were tolerant to the inhibitors.

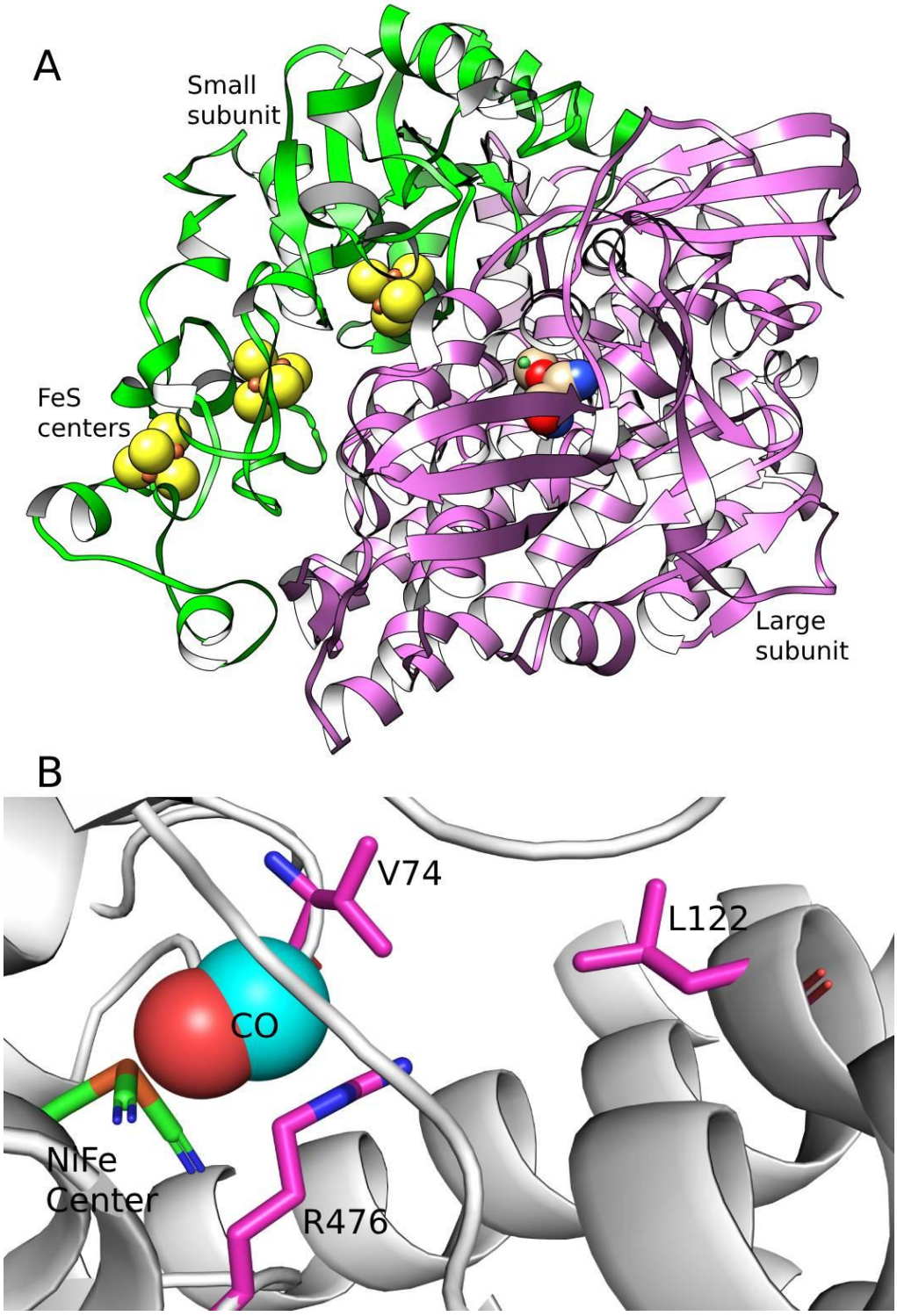

Figure 1. Structure of [NiFe] hydrogenase (PDB 1YQW)[33]. A) Small (green ribbon) and large (pink ribbon) subunits, and the positions of the metal centers (3 FeS centers in the small subunit, and the active site in the large subunit). B) The active site of [NiFe] hydrogenase. Selected residues and metals of the active site are shown in stick representation, CO is shown with spheres. Previous works suggested that two pairs of residues (74 and 122, and 74 and 476) were the main bottlenecks for gas diffusion.

Understanding the role of the mutations in the diffusion of the ligands through the tunnels and how they change the binding and unbinding pathways can give us insights on how to engineer tolerant mutants. Such pathways cannot be observed experimentally, but they can be studied using computational methods. One of the computational approaches to observe binding and unbinding pathways is molecular dynamics (MD) simulations. MD employs Newton's laws to propagate the motions of atoms in a system, allowing one to investigate the motions of biomacromolecules[34]. However, one of the main limitations of this method has been the timescales that can be achieved. Binding and unbinding events of small molecules happen in the microsecond timescale or slower, while conventional MD (cMD) simulations are usually limited to tens of microseconds[35]. Therefore, it is not feasible to simulate binding events with cMD. In recent years, many enhanced sampling methods have been developed that can be employed to sample binding and unbinding events in the time scales achieved by cMD[35–38]. τRAMD (τ-Random Accelerated Molecular Dynamics) is an enhanced sampling method in which a force of constant magnitude and random orientation is applied to the center of mass (COM) of the ligand molecule, increasing the chances of observation of unbinding events[39]. τRAMD provides relative residence time values, which can be used to distinguish slow unbinding ligands from fast unbinding ligands and rank them accordingly. τRAMD has been used to investigate ligand unbinding in several systems, such as T4 lysozyme mutants, kinases and heat shock protein 90, and it was able to reproduce experimental kinetic rates[40–43].

Several works have studied the [NiFe] hydrogenase by computational methods, providing mechanistic insights about the diffusion of gas molecules inside the tunnels[44–54]. Wang et al.[45,49] developed a master equation for calculation of gas diffusion rates within the [NiFe] hydrogenase, and used their method to further understand gas diffusion in the mutants designed by Liebgott et al.[32] Based on their results, they proposed that, in addition to the distance between

residues 74 and 122, the distance between residues 74 and 476 (Figure 1B) is also a bottleneck that controls gas diffusion in the [NiFe] hydrogenase of *Desulfovibrio fructosovorans.* Additionally, they also proposed that mutations in the position 476 could lead to resistance to CO and O_2. However, such a proposition could not be tested, because R476 is essential for the catalytic activity of [NiFe] hydrogenase.

In this work, we focused on the wild type form and 10 mutants of [NiFe] hydrogenase from *Desulfovibrio fructosovorans* reported by Liebgott et al[32]. We employed the enhanced sampling method τRAMD to obtain unbinding events of the substrate (H_2) and inhibitors (O_2 and CO) in order to understand the mechanism of diffusion of these gas molecules through the 30 Å long tunnels of this enzyme. The relative residence times computed with τRAMD for CO are in agreement with the experimental ones. We found that the residence time is mainly controlled by the bottleneck between residues 74 and 122 (Figure 1B). We computed pathway probabilities for the unbinding of different gas molecules and we observed that, while the most probable pathways are the same for different gas molecules and different mutants, the secondary pathways can be different. Finally, we propose that blockage of the main paths in combination with opening of the main secondary path used by H_2, can be a feasible strategy to achieve CO and O_2 resistance in the [NiFe] hydrogenase from *Desulfovibrio fructosovorans.*

Computational Methods

There are a total of 10 [NiFe] hydrogenase mutants that have experimental kinetic rates determined for CO (Table S1), and 4 mutants with experimental kinetic rates determined for O_2[32]. Additionally, kinetic rates are available for CO in complex with the wild type (WT) [NiFe] hydrogenase. For the substrate (H_2), there are only experimental Michaelis constants available[32]. We studied a total of 13 complexes, 10 [NiFe] hydrogenase mutants and the WT [NiFe] hydrogenase in complex with CO, and also the WT [NiFe] hydrogenase in complex with O_2 and H_2 (Table S1). Since experimental kinetic rates were not available for most of the mutants in complex with O_2 or H_2, we only investigated the WT [NiFe] hydrogenase in complex with O_2 and H_2.

The WT [NiFe] hydrogenase from *Desulfovibrio fructosovorans* and the mutants V74M and V74M L122M had crystal structures available (PDB IDs 1YQW[33], 3H3X[55] and 3CUR[28],

respectively). The structures were used to model the protein-ligand complex. The peroxide ion in the structures was replaced by the gas molecule simulated (H_2, CO or O_2). In the case of CO, the O atom was put close to the [NiFe] metal center. For the rest of the mutations, the crystal structure of the WT [NiFe] hydrogenase was used as a starting model, and the rotamer tool in UCSF chimera software[56,57] was used to make point mutations on the 74 or 122 positions of the large subunit of the enzyme. Then, the protonation states of the residues for all mutants at pH 7, the pH used for measuring experimental kinetic rates[32], were determined using Propka version 3.5.2[58–60], as implemented in the program pdb2pqr version 2.1.1[61,62].

All the MD simulations were carried out using GROMACS-RAMD version 2.0[39,63] and the AMBER99SB force field[64]. In order to describe the metal sites of the [NiFe] hydrogenase, the force field bonded parameters and the partial charges of the metal centers were obtained from the works of Smith et al.[44] and Teixeira et al.[65], respectively. The parameters were selected based on the state of the metal centers. We selected the reduced state for the [FeS] centers and the NiB state for the [NiFe] center. The force field parameters of the gas molecules (H_2, CO, O_2) were obtained from the literature or from quantum mechanical (QM) calculations. For O_2 and H_2, the bonded parameters and the partial charges were obtained from Wang et al[66]. For CO, the bonded parameters were obtained from the work of Straub et al.[67]. For the partial charges of CO, we performed QM calculations using Gaussian[68], Hartree Fock and the 6-31G* basis set, which resulted in partial charges of +0.059 e for C and -0.059 e for O, respectively (Table S2).

The protein-ligand complex was placed in the center of a cubic box with a distance of 1 nm from all edges and solvated with the TIP3P[69] water model. Then, sodium and chloride ions were added to produce an ionic strength of 118 mM. The ionic strength was adopted to reproduce the conditions used for the protein film voltammetry experiments to obtain kinetic rates[32]. The final systems had ~113000 atoms.

Next, we performed energy minimization and a 50 ns cMD simulation for each starting structure (details below). The gas molecules were positionally restrained with a harmonic force constant of 5000 $kJ/mol^{-1}nm^{-2}$ in order to keep them inside the active site. Then, the end frame of the 50 ns cMDs were used to run 5 replicas of cMD, each with a duration of 20 ns. The 5 replicas were performed to increase diversity among the structures. The end frame of each replica was

then used as the starting structure of the τRAMD runs. For each replica, we performed 15 τRAMD simulations to achieve a total of 75 dissociation events for each mutation.

The starting structure was energy minimized using the steepest descent algorithm until the maximum force was less than 10 kJ $mol^{-1}.nm^{-1}$. Then, the system was heated to 310 K using the Berendsen thermostat[70]. Next, the pressure was equilibrated to 1 bar using the Berendsen barostat[70]. After temperature and pressure equilibration, additional steps were performed to reduce the positional restraints over the system's heavy atoms in 4 steps (500, 200, 50 and 0 $kJ/mol^{-1}nm^{-2}$, but 5000 $kJ/mol^{-1}nm^{-2}$ positional restraints on the ligand atoms were kept in all simulations, except the τRAMD unbinding simulation runs). In all simulations, after equilibration, temperature and pressure coupling were achieved with the Nose-Hoover thermostat[71,72] and the Parrinello-Rahman barostat, respectively[73,74]. The covalent bonds to hydrogen atoms were constrained using the Linear Constraint Solver (LINCS) algorithm to maintain constant bond lengths[75]. Bond lengths for the solvent were constrained using the SETTLE algorithm[76]. The long-range electrostatic interactions were treated using the Particle Mesh Ewald (PME) method with a real-space cutoff of 1.2 nm, PME order of four, and a Fourier grid spacing of 1.2 Å[77,78]. Van-der-Waals forces were computed using a cutoff of 1.2 nm. The magnitude of the force for the τRAMD runs was set to 1 kcal/molÅ, the threshold distance was set to 0.0025 nm and the evaluation frequency was set to 100 fs. The procedure to choose the force magnitude will be explained in the results section.

Equation 1 shows the process of association and dissociation of CO to/from the enzyme (E), as observed in the experiments of Liebgott et al[32]. In CO-E, CO is covalently bound to the NiFe center. The geminate state (G) represents the state where the gas molecule is close to the NiFe center but not covalently bound to it. The k_{out} values derived from experiments[32] represent the rate in which the gas molecule goes from the bound state (CO-E), where CO is covalently bound to the NiFe center, to the unbound state (CO + E), in which the CO molecule is free in the solvent. However, in our dissociation trajectories, since we are using a classical force field, we did not simulate the rupture of the covalent bond between CO and the [NiFe] center. The values obtained from simulations represent k_{-1}. Previous work[32] has presented and discussed evidence that changes in the k_{out} values are mainly due to changes in the k_{-1} values for the different mutants of [NiFe] hydrogenase studied by Liebgott et al.[32] and investigated here. Along the

paper, we discuss the diffusion of gas molecules in terms of residence time ($1/k_{out}$ for experiments, $1/k_{-1}$ for simulations).

$$CO + E \underset{k_{-1}}{\overset{k_{+1}}{\rightleftharpoons}} G \underset{k_{-2}}{\overset{k_{+2}}{\rightleftharpoons}} CO\text{-}E \quad (1)$$

Analyses of dissociation trajectories were performed using GROMACS utilities and UCSF Chimera[56]. Analysis of the tunnels was performed using CAVER 3.0, Pymol 2.0 and AQUA-DUCT 1.0[79–81]. The parameters used for analysis are provided in the supplementary information.

Results & Discussion

tauRAMD can discriminate complexes with short and long residence times

The main parameter to be optimized in τRAMD is the magnitude of the random force applied on the COM of the gas molecule to enhance dissociation. The magnitude of the force has a direct effect on the speed of the unbinding process. If the force is too high, it will result in a very fast unbinding event, which could lead to reduced sampling of the transition state. We found that 1 kcal/molÅ of force magnitude is optimum for our case, providing a good compromise between force magnitude and computational time to sample unbinding events (Figure S1, Table S3). Moreover, the force of 1 kcal/molÅ provided a good discrimination between the kinetic rates of the fastest, WT-CO, and the slowest dissociating complex, V74W-CO (Figure S1, Table S3). We also tested different threshold distances (Figure S2, Table S4), which determine whether there will be a change in the orientation of the force according to the ligand displacement for a given time interval, and adopted the value of 0.0025 nm for the work.

Before the τRAMD unbinding simulation runs, we performed a 50 ns cMD run for every system to stabilize the conformation of the mutated residues, and of the residues near the mutation. Then, we used the final snapshot to perform five 20 ns cMD (replicas) in order to explore the conformational space. The end frames of the five replicas were used as the initial structures for the subsequent τRAMD simulations. Figure 2 and Table S1 show the experimental and computed RT values for CO in complex with WT and 10 different mutants. We achieved a Pearson correlation coefficient (R) of 0.62 and a Spearman's rank correlation coefficient (ρ) of 0.57. The R and ρ values are reasonable, and allow one to discriminate complexes with long and short RT. It is worth mentioning that, if outliers (V74N and V74Q) are excluded, an R of 0.71 and a ρ of 0.75 are achieved. Data analysis and discussion refer to all the data points presented in Figure 2.

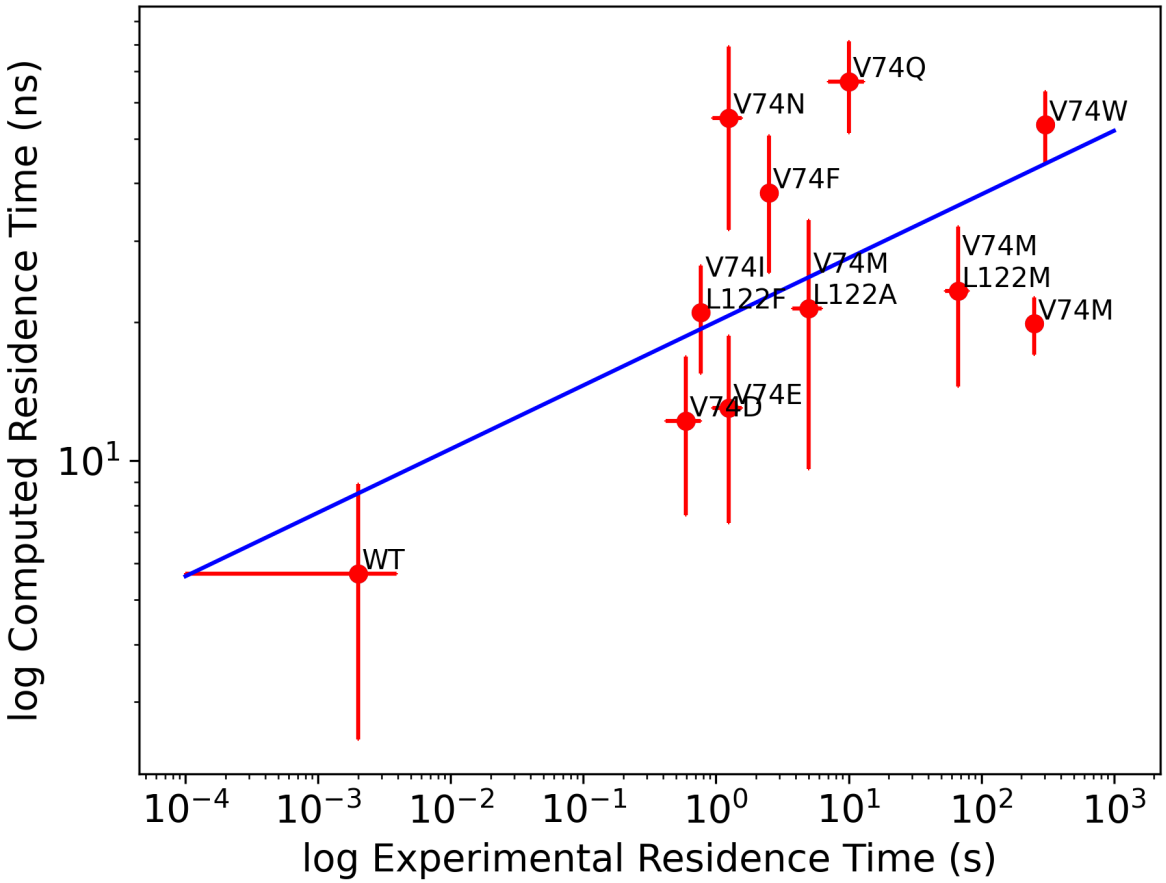

Figure 2. Comparison between experimental and computed residence times of CO in complex with wild type (WT) or mutants of [NiFe] hydrogenase using τRAMD with 1 kcal/molÅ of force magnitude (R = 0.62, ρ = 0.57). If outliers (V74N and V74Q) are excluded, a higher correlation is achieved (R = 0.71, ρ = 0.75). Data can be found in Table S1.

The bottleneck between residues 74 and 122 modulates residence times for CO

As stated in the introduction, two bottlenecks were proposed previously as the main factors modulating the diffusion of gas molecules inside [NiFe] hydrogenase, the distance between residues 74 and 122, and the distance between residues 74 and 476. We calculated the width of these two bottlenecks by calculating the distance between the side chain terminal carbon atoms of the investigated residues (Table S5). The distribution of the distances is presented in Figures 3A and 3B. The distances found in the crystal structures are shown as dashed lines. For the 74-122 bottleneck, it can be seen that the distances found in the simulations fluctuate around

the values found in the crystal structures for the mutants V74M and V74M-L122M, while the distances found in the simulations are larger than the distance observed in the crystal structure of the WT [NiFe] hydrogenase. This observation showcases the importance of considering dynamics and flexibility to investigate tunnels and ligand dissociation. The correlation between the width of the 74-122 bottleneck and RT is strongly negative, showing that the longer the RT, the narrower the width of the 74-122 bottleneck (R = -0.71, Figure 3C). This shows that the 74-122 bottleneck is effectively regulating RT values and CO dissociation in [NiFe] hydrogenase. This result is in disagreement with previous computational work from Wang et al.[49], which did not find a clear correlation between the width of the 74-122 bottleneck and RT values for the mutants of [NiFe] hydrogenase. Possible explanations could be the longer simulations or the larger number of mutants considered in the present work.

The correlation between the width of the 74-476 bottleneck and RT is positive (R = 0.63, Figure 3D), showing that the longer the RT, the wider the width of the 74-476 bottleneck. Therefore, we found no evidence that the distance between residues 74 and 476 acts as a bottleneck for CO dissociation in the mutants investigated. We hypothesize that bulky residues at position 74 cannot fit properly in the free space available in the tunnel and the positive correlation found is due to the bulkiness of the residues or, in the case of the M mutation, high fluctuations of the flexible residue.

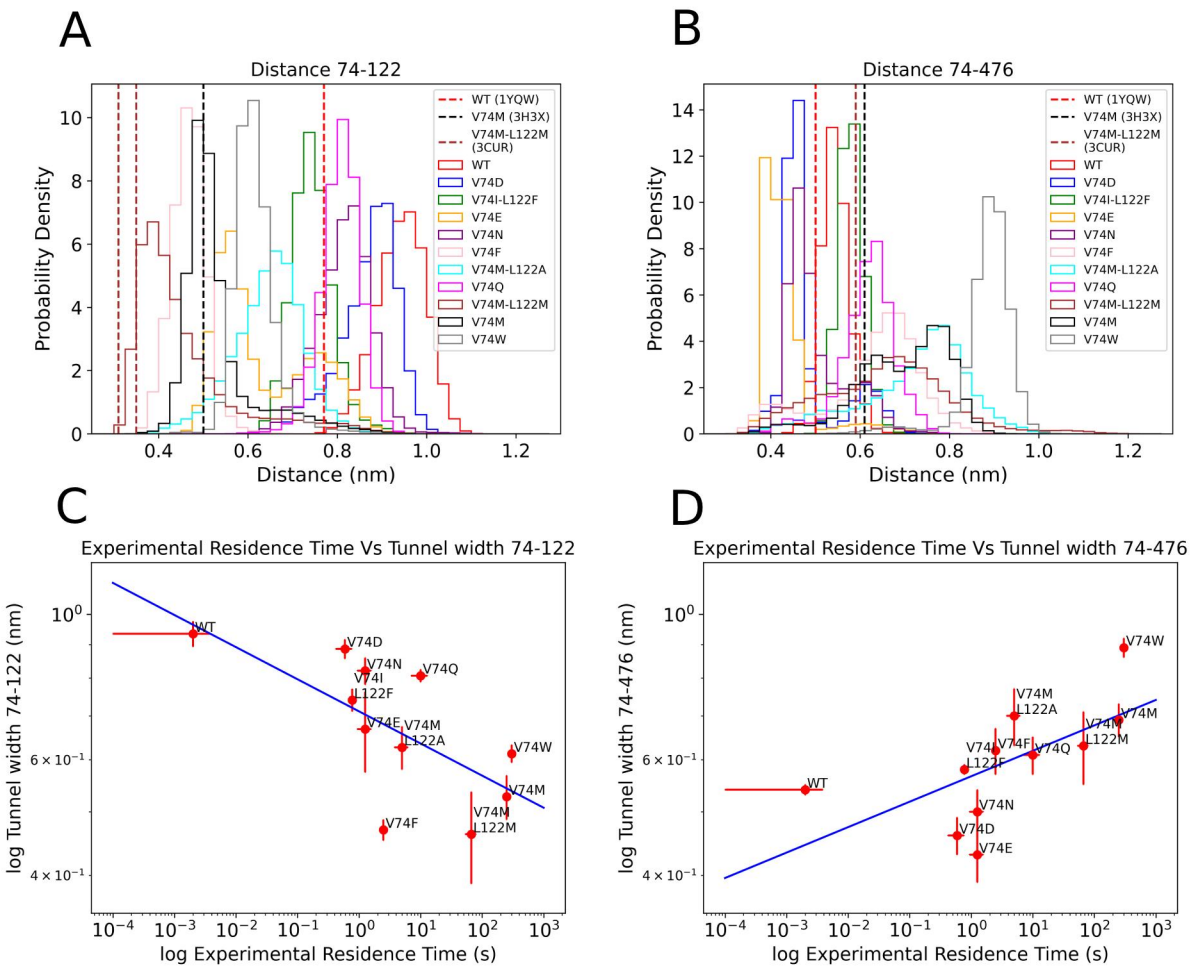

Figure 3. Distribution of the widths of the two bottlenecks and correlation with experimental residence times (RT). A) Distribution of the widths of the 74-122 bottleneck in different mutants of [NiFe] hydrogenase and B) distribution of the widths of the 74-476 bottleneck in different mutants of [NiFe] hydrogenase. The atoms used to calculate the distances can be found in Table S5. The widths of the bottlenecks in the three crystallographic structures (PDB ID 1YQW, 3H3X, 3CUR for WT, V74M and V74M-L122M, respectively) are shown as dashed lines. C) Correlation between experimental RT values and the average width of the 74-122 bottleneck in different mutants of [NiFe] hydrogenase (R = -0.71) and D) correlation between experimental RT values and the average width of the 74-476 bottleneck in different mutants of [NiFe] hydrogenase (R = 0.63). The widths of the bottlenecks were calculated using the entire τRAMD dissociation trajectories in all mutants.

In order to understand the diffusion of CO inside the tunnels before leaving them through the exit point, we calculated the time it takes for CO to lose contact with the residues at positions 74 and 122. We found that, on average, CO stays in the tunnels for about 4 ns after losing contact with residues 74 and 122 (Table S6). The variation in RT values in simulations of different [NiFe] hydrogenase mutants is mostly dictated by the time it takes CO to pass the 74-122 bottleneck, which is another evidence of the importance of this bottleneck for modulating RT values in [NiFe] hydrogenase.

Paths T1 and T2 are the preferred paths for unbinding

We mapped the tunnels connecting the active site to the solvent in the crystallographic structure of the WT [NiFe] hydrogenase (PDB ID 1YQW)[33] using CAVER 3.0[79] and found 9 different tunnels (Figure 4A). By analyzing the tunnels, we found that the starting points of them can be divided into two major groups. As it is shown in Figure 4B, most of the tunnels (T1, T2, T5, T6 and T7) go through the 74-122 bottleneck, while some tunnels (T3, T4, T8 and T9) skip the 74-122 bottleneck.

We identified 9 different pathways by tracking the motion of CO in the unbinding trajectories using AQUA-DUCT 1.0[80]. These 9 paths from the trajectories are associated with the 9 tunnels identified in the crystallographic structure, showing that CO can use all of these 9 different tunnels for unbinding. Figure 5 shows the population of the unbinding pathways of CO in different mutants. The most frequently used pathways are through the T1 and T2 tunnels in all of the mutants. The T1 and T2 tunnels both end at either side of the second α-helix of the small subunit (α2S), and the route of both tunnels is the same until they reach this helix. Our results suggest that the exit points of T1, T2 and T7 are controlled by the α2S, α7L and α7S α-helices (Figure 4A). It is interesting to note that, in mutants with longer residence times and more restriction for CO diffusion, there is an increase in the utilization of secondary or alternative exit paths, such as path T8. It is also important to mention that CO can move between pathways and diffuse in the tunnels until ultimately fully getting out of the enzyme. The unbinding pathways and populations presented in figure 5 are associated with the last path accessed by CO before it left the interior of the enzyme.

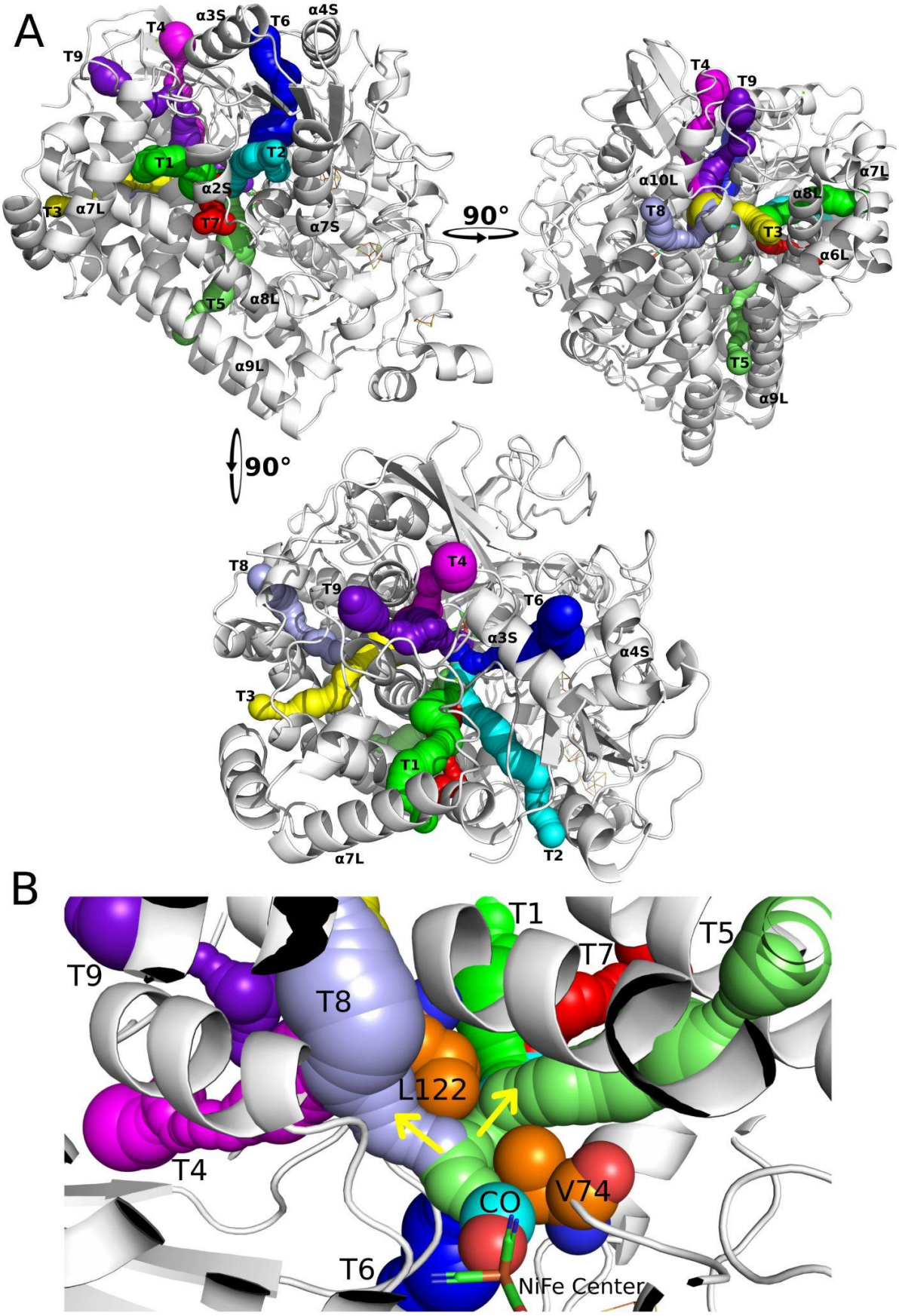

Figure 4. Tunnels and unbinding pathways for CO identified in the [NiFe] hydrogenase A) Nine tunnels (T1-T9) were identified inside the crystallographic structure of the WT [NiFe] hydrogenase (PDB ID 1YQW)[33] using the CAVER 3.0 plugin in Pymol[79,81]. The secondary structures are named according to order of appearance in the primary structure and subunits (S for small, L for large). Example: α2S, 2nd α-helix from the small subunit. The gas molecules used these tunnels as unbinding pathways in the trajectories. B) The course of the tunnels is divided into two major groups, as indicated by the yellow arrows. Note that T3, T4, T8 and T9 skip the 74-122 bottleneck, and T1, T2, T5, T6 and T7 go through the 74-122 bottleneck. Residues V74 and L122 are represented as orange spheres.

The pathways identified here are in qualitative agreement with previous works which investigated pathways of gas molecules inside the [NiFe] hydrogenase of *Desulfovibrio fructosovorans*. It has been reported that there is a "VA"-shaped set of gas tunnels connecting the catalytic site to the surface of the enzyme[45,48]. This "VA"-shaped tunnel corresponds to tunnels T1, T2, T3, T5 and T7 characterized here. Wang et al.[45] reported that in addition to the "VA"-shaped tunnels, they have identified 2 more pathways for H_2, O_2 and CO to reach the catalytic site that skip the 74-122 bottleneck, which is in agreement with our results. Oteri et al.[46] investigated the diffusion pathways of H_2 from the enzyme surface to the catalytic site using MD and Brownian Dynamics simulations. They presented the five most frequent tunnels, which are consistent with the tunnels identified in our work. Additionally, Kalms et al.[47], using simulations of the [NiFe] hydrogenase from *Ralstonia eutropha*, reported 2 tunnels, A and B. Tunnel A corresponds to T1, T2 and T7, and tunnel B corresponds to T3, T5 and T8.

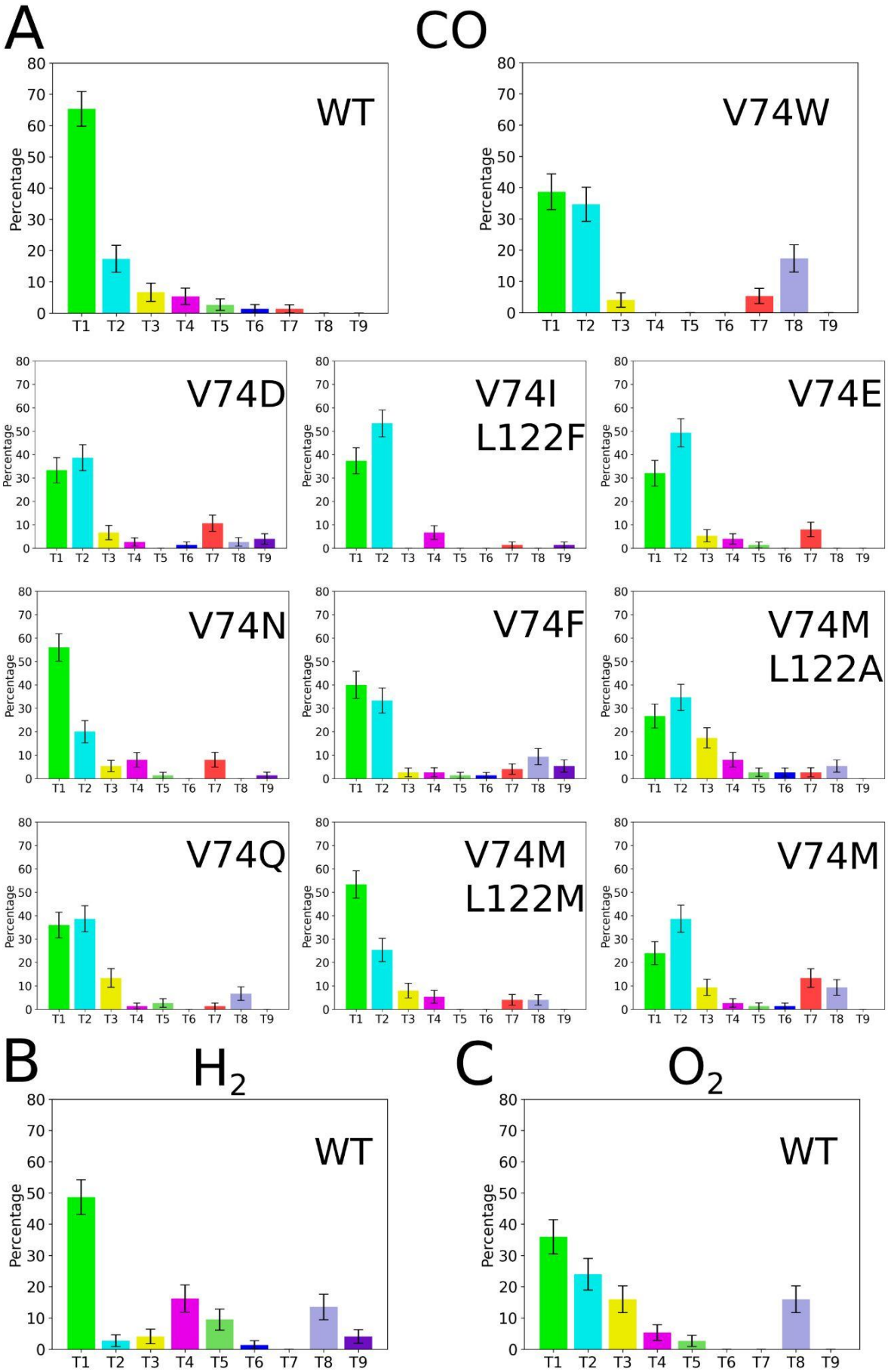

Figure 5. Populations of different pathways that CO, H_2 and O_2 use for unbinding from different mutants of [NiFe] hydrogenase. The colors of the paths match the colors of the associated tunnels in Figure 4A. The standard deviation on each bar comes from bootstrapping analysis. A) CO complexes, WT-CO with the shortest RT, and the V74W-CO complex, with the longest RT, are shown on top. Below, the other CO-mutant complexes are shown from the one with the shortest RT (up left corner) to the one with the longest RT (right down corner). B) H_2-WT and C) O_2-WT complexes. Unbinding pathways were obtained from τRAMD dissociation trajectories and identified using AQUA-DUCT 1.0[80].

Different gas molecules use different secondary paths for unbinding

In addition to CO, we also performed τRAMD simulations to study the unbinding pathways of O_2 and H_2 from the WT [NiFe] hydrogenase (Table S1). We found that, similar to CO, paths T1 and T2 are the most frequently used pathways for O_2 and H_2 unbinding (Figure 5). However, the secondary paths used by the different gas molecules are different. While CO has a low probability of utilization of secondary pathways during unbinding from the WT [NiFe] hydrogenase (less than 10% population for paths different from T1 and T2), O_2 uses paths T3 and T8 more frequently, while H_2 uses paths T4 and T8 more frequently. Therefore, we propose that mutations to block the main paths, T1 and T2, in combination with mutations to open one of the main secondary paths used by H_2, T4, can be a feasible strategy to achieve CO and O_2 resistance in the [NiFe] hydrogenase from *Desulfovibrio fructosovorans*.

Different reasons may explain why the three gas molecules have different preferences concerning secondary paths for unbinding. In the case of O_2, since it is the biggest gas molecule among the three, we hypothesize that avoidance of the 74-122 bottleneck can be the reason why the population of the pathways which skip this bottleneck, such as paths T4 and T8, is higher. We can also see this behavior for CO in the V74W, V74F and V74Q mutants, in which the width of the 74-122 bottleneck is the shortest (Figure 3 and Figure 5). In the case of H_2, we hypothesize that the higher mobility of the smallest gas molecule among the three can be the reason why H_2 can use pathways with low populations for the other gas molecules, like path T4.

Conclusion

The hydrogenase family of enzymes are of technological importance, since they can be used for clean energy production. However, some of the members of this family of enzymes that have high catalytic rates, such as the [NiFe] hydrogenase from *Desulfovibrio fructosovorans*, have been evolved in anaerobic environments and exposure to gas molecules present in the atmosphere, such as O_2 and CO, can inhibit or damage the catalytic site, limiting their use in biofuel cells. One strategy to get around this problem is to engineer this enzyme to be O_2 and CO-resistant by introducing point mutations to block the access of inhibitors to the catalytic site. Herein, we studied the unbinding pathways of CO in complex with 10 different mutants of [NiFe] hydrogenase using τRAMD. While previous works proposed the existence of two bottlenecks (residues 74-122, and residues 74-476) to control gas diffusion, we found evidence that only one of these bottlenecks, the 74-122 bottleneck, effectively modulates the dissociation rates of CO in the mutants simulated. We also identified 9 different tunnels connecting the catalytic site to the surface of the enzyme. We found that, while the most utilized paths for dissociation from the WT [NiFe] hydrogenase are the same for H_2, CO and O_2, the secondary paths change for the different gas molecules, offering an opportunity for the rational design O_2- and CO-tolerant mutants of [NiFe] hydrogenase. We propose that mutations to block the main paths, T1 and T2, in combination with mutations to open one of the main secondary paths used by H_2, T4, can be a feasible strategy to achieve CO and O_2 resistance in the [NiFe] hydrogenase from *Desulfovibrio fructosovorans*.

Supporting Information

Supporting information (Tables S1-S6, Figures S1-S2) is available free of charge.

Additional supporting information is available in the link below (sample mdp files to run molecular dynamics simulations; modified force field files, including parameters for the metal centers in [NiFe] hydrogenase and parameters for the gas molecules; structures used to start simulations; Pymol session with the nine tunnels identified): https://doi.org/10.5281/zenodo.10412859.

Acknowledgements

Funding from DFG under Germany's Excellence Strategy – EXC 2008/1-390540038 – UniSysCat is gratefully acknowledged. The authors also gratefully acknowledge the Gauss

Centre for Supercomputing e.V. (www.gauss-centre.eu) for funding this project by providing computing time through the John von Neumann Institute for Computing (NIC) on the GCS Supercomputer JUWELS at Jülich Supercomputing Centre (JSC).

References

(1) Lubitz, W.; Ogata, H.; Rüdiger, O.; Reijerse, E. Hydrogenases. *Chem. Rev.* **2014**, *114* (8), 4081–4148. https://doi.org/10.1021/cr4005814.
(2) Simmons, T. R.; Berggren, G.; Bacchi, M.; Fontecave, M.; Artero, V. Mimicking Hydrogenases: From Biomimetics to Artificial Enzymes. *Coord. Chem. Rev.* **2014**, *270–271*, 127–150. https://doi.org/10.1016/j.ccr.2013.12.018.
(3) Cox, N.; Pantazis, D. A.; Neese, F.; Lubitz, W. Artificial Photosynthesis: Understanding Water Splitting in Nature. *Interface Focus* **2015**, *5* (3), 20150009. https://doi.org/10.1098/rsfs.2015.0009.
(4) Nagy, V.; Podmaniczki, A.; Vidal-Meireles, A.; Tengölics, R.; Kovács, L.; Rákhely, G.; Scoma, A.; Tóth, S. Z. Water-Splitting-Based, Sustainable and Efficient H2 Production in Green Algae as Achieved by Substrate Limitation of the Calvin–Benson–Bassham Cycle. *Biotechnol. Biofuels* **2018**, *11* (1), 69. https://doi.org/10.1186/s13068-018-1069-0.
(5) U.S. Hands out $7 Billion for Hydrogen Hubs, 2023. https://doi.org/10.1126/science.adl3664.
(6) Stripp, S. T.; Duffus, B. R.; Fourmond, V.; Léger, C.; Leimkühler, S.; Hirota, S.; Hu, Y.; Jasniewski, A.; Ogata, H.; Ribbe, M. W. Second and Outer Coordination Sphere Effects in Nitrogenase, Hydrogenase, Formate Dehydrogenase, and CO Dehydrogenase. *Chem. Rev.* **2022**, *122* (14), 11900–11973. https://doi.org/10.1021/acs.chemrev.1c00914.
(7) Fisher, H. F.; Krasna, A. I.; Rittenberg, D. The Interaction of Hydrogenase with Oxygen. *J. Biol. Chem.* **1954**, *209* (2), 569–578. https://doi.org/10.1016/S0021-9258(18)65483-3.
(8) Stiebritz, M. T.; Reiher, M. Hydrogenases and Oxygen. *Chem. Sci.* **2012**, *3* (6), 1739. https://doi.org/10.1039/c2sc01112c.
(9) Baffert, C.; Bertini, L.; Lautier, T.; Greco, C.; Sybirna, K.; Ezanno, P.; Etienne, E.; Soucaille, P.; Bertrand, P.; Bottin, H.; Meynial-Salles, I.; De Gioia, L.; Léger, C. CO Disrupts the Reduced H-Cluster of FeFe Hydrogenase. A Combined DFT and Protein Film Voltammetry Study. *J. Am. Chem. Soc.* **2011**, *133* (7), 2096–2099. https://doi.org/10.1021/ja110627b.
(10) Pandelia, M.-E.; Ogata, H.; Currell, L. J.; Flores, M.; Lubitz, W. Inhibition of the [NiFe] Hydrogenase from Desulfovibrio Vulgaris Miyazaki F by Carbon Monoxide: An FTIR and EPR Spectroscopic Study. *Biochim. Biophys. Acta BBA - Bioenerg.* **2010**, *1797* (2), 304–313. https://doi.org/10.1016/j.bbabio.2009.11.002.
(11) Cracknell, J. A.; Wait, A. F.; Lenz, O.; Friedrich, B.; Armstrong, F. A. A Kinetic and Thermodynamic Understanding of O_2 Tolerance in [NiFe]-Hydrogenases. *Proc. Natl. Acad. Sci.* **2009**, *106* (49), 20681–20686. https://doi.org/10.1073/pnas.0905959106.
(12) Lukey, M. J.; Roessler, M. M.; Parkin, A.; Evans, R. M.; Davies, R. A.; Lenz, O.; Friedrich, B.; Sargent, F.; Armstrong, F. A. Oxygen-Tolerant [NiFe]-Hydrogenases: The Individual and Collective Importance of Supernumerary Cysteines at the Proximal Fe-S Cluster. *J. Am. Chem. Soc.* **2011**, *133* (42), 16881–16892. https://doi.org/10.1021/ja205393w.
(13) Liebgott, P.-P.; De Lacey, A. L.; Burlat, B.; Cournac, L.; Richaud, P.; Brugna, M.; Fernandez, V. M.; Guigliarelli, B.; Rousset, M.; Léger, C.; Dementin, S. Original Design of an Oxygen-Tolerant [NiFe] Hydrogenase: Major Effect of a Valine-to-Cysteine Mutation near the Active Site. *J. Am. Chem. Soc.* **2011**, *133* (4), 986–997.

https://doi.org/10.1021/ja108787s.
(14) Abou Hamdan, A.; Liebgott, P.-P.; Fourmond, V.; Gutiérrez-Sanz, O.; De Lacey, A. L.; Infossi, P.; Rousset, M.; Dementin, S.; Léger, C. Relation between Anaerobic Inactivation and Oxygen Tolerance in a Large Series of NiFe Hydrogenase Mutants. *Proc. Natl. Acad. Sci.* **2012**, *109* (49), 19916–19921. https://doi.org/10.1073/pnas.1212258109.
(15) Del Barrio, M.; Guendon, C.; Kpebe, A.; Baffert, C.; Fourmond, V.; Brugna, M.; Léger, C. Valine-to-Cysteine Mutation Further Increases the Oxygen Tolerance of *Escherichia Coli* NiFe Hydrogenase Hyd-1. *ACS Catal.* **2019**, *9* (5), 4084–4088. https://doi.org/10.1021/acscatal.9b00543.
(16) Liebgott, P.-P.; Dementin, S.; Léger, C.; Rousset, M. Towards Engineering O_2-Tolerance in [Ni–Fe] Hydrogenases. *Energy Env. Sci* **2011**, *4* (1), 33–41. https://doi.org/10.1039/C0EE00093K.
(17) Lautier, T.; Ezanno, P.; Baffert, C.; Fourmond, V.; Cournac, L.; Fontecilla-Camps, J. C.; Soucaille, P.; Bertrand, P.; Meynial-Salles, I.; Léger, C. The Quest for a Functional Substrate Access Tunnel in FeFe Hydrogenase. *Faraday Discuss* **2011**, *148*, 385–407. https://doi.org/10.1039/C004099C.
(18) Radu, V.; Frielingsdorf, S.; Evans, S. D.; Lenz, O.; Jeuken, L. J. C. Enhanced Oxygen-Tolerance of the Full Heterotrimeric Membrane-Bound [NiFe]-Hydrogenase of *Ralstonia Eutropha*. *J. Am. Chem. Soc.* **2014**, *136* (24), 8512–8515. https://doi.org/10.1021/ja503138p.
(19) Fritsch, J.; Lenz, O.; Friedrich, B. Structure, Function and Biosynthesis of O2-Tolerant Hydrogenases. *Nat. Rev. Microbiol.* **2013**, *11* (2), 106–114. https://doi.org/10.1038/nrmicro2940.
(20) Friedrich, B.; Fritsch, J.; Lenz, O. Oxygen-Tolerant Hydrogenases in Hydrogen-Based Technologies. *Curr. Opin. Biotechnol.* **2011**, *22* (3), 358–364. https://doi.org/10.1016/j.copbio.2011.01.006.
(21) Goris, T.; Wait, A. F.; Saggu, M.; Fritsch, J.; Heidary, N.; Stein, M.; Zebger, I.; Lendzian, F.; Armstrong, F. A.; Friedrich, B.; Lenz, O. A Unique Iron-Sulfur Cluster Is Crucial for Oxygen Tolerance of a [NiFe]-Hydrogenase. *Nat. Chem. Biol.* **2011**, *7* (5), 310–318. https://doi.org/10.1038/nchembio.555.
(22) Kokkonen, P.; Bednar, D.; Pinto, G.; Prokop, Z.; Damborsky, J. Engineering Enzyme Access Tunnels. *Biotechnol. Adv.* **2019**, *37* (6), 107386. https://doi.org/10.1016/j.biotechadv.2019.04.008.
(23) Pavlova, M.; Klvana, M.; Prokop, Z.; Chaloupkova, R.; Banas, P.; Otyepka, M.; Wade, R. C.; Tsuda, M.; Nagata, Y.; Damborsky, J. Redesigning Dehalogenase Access Tunnels as a Strategy for Degrading an Anthropogenic Substrate. *Nat. Chem. Biol.* **2009**, *5* (10), 727–733. https://doi.org/10.1038/nchembio.205.
(24) Lu, Z.; Li, X.; Zhang, R.; Yi, L.; Ma, Y.; Zhang, G. Tunnel Engineering to Accelerate Product Release for Better Biomass-Degrading Abilities in Lignocellulolytic Enzymes. *Biotechnol. Biofuels* **2019**, *12* (1), 275. https://doi.org/10.1186/s13068-019-1616-3.
(25) Cano, M.; Volbeda, A.; Guedeney, G.; Aubert-Jousset, E.; Richaud, P.; Peltier, G.; Cournac, L. Improved Oxygen Tolerance of the Synechocystis Sp. PCC 6803 Bidirectional Hydrogenase by Site-Directed Mutagenesis of Putative Residues of the Gas Diffusion Channel. *Int. J. Hydrog. Energy* **2014**, *39* (30), 16872–16884. https://doi.org/10.1016/j.ijhydene.2014.08.030.
(26) Banerjee, R.; Lipscomb, J. D. Small-Molecule Tunnels in Metalloenzymes Viewed as Extensions of the Active Site. *Acc. Chem. Res.* **2021**, *54* (9), 2185–2195. https://doi.org/10.1021/acs.accounts.1c00058.
(27) Gora, A.; Brezovsky, J.; Damborsky, J. Gates of Enzymes. *Chem. Rev.* **2013**, *113* (8), 5871–5923. https://doi.org/10.1021/cr300384w.
(28) Leroux, F.; Dementin, S.; Burlat, B.; Cournac, L.; Volbeda, A.; Champ, S.; Martin, L.;

Guigliarelli, B.; Bertrand, P.; Fontecilla-Camps, J.; Rousset, M.; Léger, C. Experimental Approaches to Kinetics of Gas Diffusion in Hydrogenase. *Proc. Natl. Acad. Sci.* **2008**, *105* (32), 11188–11193. https://doi.org/10.1073/pnas.0803689105.
(29) Meng, S.; An, R.; Li, Z.; Schwaneberg, U.; Ji, Y.; Davari, M. D.; Wang, F.; Wang, M.; Qin, M.; Nie, K.; Liu, L. Tunnel Engineering for Modulating the Substrate Preference in Cytochrome P450BsβHI. *Bioresour. Bioprocess.* **2021**, *8* (1), 26. https://doi.org/10.1186/s40643-021-00379-1.
(30) Kaushik, S.; Marques, S. M.; Khirsariya, P.; Paruch, K.; Libichova, L.; Brezovsky, J.; Prokop, Z.; Chaloupkova, R.; Damborsky, J. Impact of the Access Tunnel Engineering on Catalysis Is Strictly Ligand‐specific. *FEBS J.* **2018**, *285* (8), 1456–1476. https://doi.org/10.1111/febs.14418.
(31) Buhrke, T.; Lenz, O.; Krauss, N.; Friedrich, B. Oxygen Tolerance of the H2-Sensing [NiFe] Hydrogenase from Ralstonia Eutropha H16 Is Based on Limited Access of Oxygen to the Active Site. *J. Biol. Chem.* **2005**, *280* (25), 23791–23796. https://doi.org/10.1074/jbc.M503260200.
(32) Liebgott, P.-P.; Leroux, F.; Burlat, B.; Dementin, S.; Baffert, C.; Lautier, T.; Fourmond, V.; Ceccaldi, P.; Cavazza, C.; Meynial-Salles, I.; Soucaille, P.; Fontecilla-Camps, J. C.; Guigliarelli, B.; Bertrand, P.; Rousset, M.; Léger, C. Relating Diffusion along the Substrate Tunnel and Oxygen Sensitivity in Hydrogenase. *Nat. Chem. Biol.* **2010**, *6* (1), 63–70. https://doi.org/10.1038/nchembio.276.
(33) Volbeda, A.; Martin, L.; Cavazza, C.; Matho, M.; Faber, B. W.; Roseboom, W.; Albracht, S. P. J.; Garcin, E.; Rousset, M.; Fontecilla-Camps, J. C. Structural Differences between the Ready and Unready Oxidized States of [NiFe] Hydrogenases. *JBIC J. Biol. Inorg. Chem.* **2005**, *10* (3), 239–249. https://doi.org/10.1007/s00775-005-0632-x.
(34) Gelpi, J.; Hospital, A.; Goñi, R.; Orozco, M. Molecular Dynamics Simulations: Advances and Applications. *Adv. Appl. Bioinforma. Chem.* **2015**, 37. https://doi.org/10.2147/AABC.S70333.
(35) Sohraby, F.; Nunes-Alves, A. Advances in Computational Methods for Ligand Binding Kinetics. *Trends Biochem. Sci.* **2023**, *48* (5), 437–449. https://doi.org/10.1016/j.tibs.2022.11.003.
(36) Nunes-Alves, A.; Kokh, D. B.; Wade, R. C. Recent Progress in Molecular Simulation Methods for Drug Binding Kinetics. *Curr. Opin. Struct. Biol.* **2020**, *64*, 126–133. https://doi.org/10.1016/j.sbi.2020.06.022.
(37) Wolf, S. Predicting Protein–Ligand Binding and Unbinding Kinetics with Biased MD Simulations and Coarse-Graining of Dynamics: Current State and Challenges. *J. Chem. Inf. Model.* **2023**, *63* (10), 2902–2910. https://doi.org/10.1021/acs.jcim.3c00151.
(38) Rydzewski, J.; Nowak, W. Ligand Diffusion in Proteins via Enhanced Sampling in Molecular Dynamics. *Phys. Life Rev.* **2017**, *22–23*, 58–74. https://doi.org/10.1016/j.plrev.2017.03.003.
(39) Kokh, D. B.; Amaral, M.; Bomke, J.; Grädler, U.; Musil, D.; Buchstaller, H.-P.; Dreyer, M. K.; Frech, M.; Lowinski, M.; Vallee, F.; Bianciotto, M.; Rak, A.; Wade, R. C. Estimation of Drug-Target Residence Times by τ-Random Acceleration Molecular Dynamics Simulations. *J. Chem. Theory Comput.* **2018**, *14* (7), 3859–3869. https://doi.org/10.1021/acs.jctc.8b00230.
(40) Nunes-Alves, A.; Kokh, D. B.; Wade, R. C. Ligand Unbinding Mechanisms and Kinetics for T4 Lysozyme Mutants from τRAMD Simulations. *Curr. Res. Struct. Biol.* **2021**, *3*, 106–111. https://doi.org/10.1016/j.crstbi.2021.04.001.
(41) Berger, B.-T.; Amaral, M.; Kokh, D. B.; Nunes-Alves, A.; Musil, D.; Heinrich, T.; Schröder, M.; Neil, R.; Wang, J.; Navratilova, I.; Bomke, J.; Elkins, J. M.; Müller, S.; Frech, M.; Wade, R. C.; Knapp, S. Structure-Kinetic Relationship Reveals the Mechanism of Selectivity of FAK Inhibitors over PYK2. *Cell Chem. Biol.* **2021**, *28* (5), 686-698.e7.

https://doi.org/10.1016/j.chembiol.2021.01.003.
(42) Kokh, D. B.; Kaufmann, T.; Kister, B.; Wade, R. C. Machine Learning Analysis of τRAMD Trajectories to Decipher Molecular Determinants of Drug-Target Residence Times. *Front. Mol. Biosci.* **2019**, *6*, 36. https://doi.org/10.3389/fmolb.2019.00036.
(43) Kokh, D. B.; Wade, R. C. G Protein-Coupled Receptor–Ligand Dissociation Rates and Mechanisms from τRAMD Simulations. *J. Chem. Theory Comput.* **2021**, *17* (10), 6610–6623. https://doi.org/10.1021/acs.jctc.1c00641.
(44) Smith, D. M. A.; Xiong, Y.; Straatsma, T. P.; Rosso, K. M.; Squier, T. C. Force-Field Development and Molecular Dynamics of [NiFe] Hydrogenase. *J. Chem. Theory Comput.* **2012**, *8* (6), 2103–2114. https://doi.org/10.1021/ct300185u.
(45) Wang, P.; Best, R. B.; Blumberger, J. Multiscale Simulation Reveals Multiple Pathways for H2 and O2 Transport in a [NiFe]-Hydrogenase. *J. Am. Chem. Soc.* **2011**, *133* (10), 3548–3556. https://doi.org/10.1021/ja109712q.
(46) Oteri, F.; Baaden, M.; Lojou, E.; Sacquin-Mora, S. Multiscale Simulations Give Insight into the Hydrogen In and Out Pathways of [NiFe]-Hydrogenases from *Aquifex Aeolicus* and *Desulfovibrio Fructosovorans*. *J. Phys. Chem. B* **2014**, *118* (48), 13800–13811. https://doi.org/10.1021/jp5089965.
(47) Kalms, J.; Schmidt, A.; Frielingsdorf, S.; Utesch, T.; Gotthard, G.; Von Stetten, D.; Van Der Linden, P.; Royant, A.; Mroginski, M. A.; Carpentier, P.; Lenz, O.; Scheerer, P. Tracking the Route of Molecular Oxygen in O_2 -Tolerant Membrane-Bound [NiFe] Hydrogenase. *Proc. Natl. Acad. Sci.* **2018**, *115* (10). https://doi.org/10.1073/pnas.1712267115.
(48) Montet, Y.; Amara, P.; Volbeda, A.; Vernede, X.; Hatchikian, E. C.; Field, M. J.; Frey, M.; Fontecilla-Camps, J. C. Gas Access to the Active Site of Ni-Fe Hydrogenases Probed by X-Ray Crystallography and Molecular Dynamics. *Nat. Struct. Biol.* **1997**, *4* (7), 523–526. https://doi.org/10.1038/nsb0797-523.
(49) Wang, P.; Blumberger, J. Mechanistic Insight into the Blocking of CO Diffusion in [NiFe]-Hydrogenase Mutants through Multiscale Simulation. *Proc. Natl. Acad. Sci.* **2012**, *109* (17), 6399–6404. https://doi.org/10.1073/pnas.1121176109.
(50) Barbosa, T. M.; Baltazar, C. S. A.; Cruz, D. R.; Lousa, D.; Soares, C. M. Studying O2 Pathways in [NiFe]- and [NiFeSe]-Hydrogenases. *Sci. Rep.* **2020**, *10* (1), 10540. https://doi.org/10.1038/s41598-020-67494-5.
(51) Topin, J.; Rousset, M.; Antonczak, S.; Golebiowski, J. Kinetics and Thermodynamics of Gas Diffusion in a NiFe Hydrogenase. *Proteins Struct. Funct. Bioinforma.* **2012**, *80* (3), 677–682. https://doi.org/10.1002/prot.23248.
(52) Wang, P.; Best, R. B.; Blumberger, J. A Microscopic Model for Gas Diffusion Dynamics in a [NiFe]-Hydrogenase. *Phys. Chem. Chem. Phys.* **2011**, *13* (17), 7708. https://doi.org/10.1039/c0cp02098b.
(53) Baltazar, C. S. A.; Teixeira, V. H.; Soares, C. M. Structural Features of [NiFeSe] and [NiFe] Hydrogenases Determining Their Different Properties: A Computational Approach. *JBIC J. Biol. Inorg. Chem.* **2012**, *17* (4), 543–555. https://doi.org/10.1007/s00775-012-0875-2.
(54) Topin, J.; Diharce, J.; Fiorucci, S.; Antonczak, S.; Golebiowski, J. O_2 Migration Rates in [NiFe] Hydrogenases. A Joint Approach Combining Free-Energy Calculations and Kinetic Modeling. *J. Phys. Chem. B* **2014**, *118* (3), 676–681. https://doi.org/10.1021/jp4093964.
(55) Dementin, S.; Leroux, F.; Cournac, L.; Lacey, A. L. D.; Volbeda, A.; Léger, C.; Burlat, B.; Martinez, N.; Champ, S.; Martin, L.; Sanganas, O.; Haumann, M.; Fernández, V. M.; Guigliarelli, B.; Fontecilla-Camps, J. C.; Rousset, M. Introduction of Methionines in the Gas Channel Makes [NiFe] Hydrogenase Aero-Tolerant. *J. Am. Chem. Soc.* **2009**, *131* (29), 10156–10164. https://doi.org/10.1021/ja9018258.
(56) Pettersen, E. F.; Goddard, T. D.; Huang, C. C.; Couch, G. S.; Greenblatt, D. M.; Meng, E. C.; Ferrin, T. E. UCSF Chimera?A Visualization System for Exploratory Research and Analysis. *J. Comput. Chem.* **2004**, *25* (13), 1605–1612. https://doi.org/10.1002/jcc.20084.

(57) Shapovalov, M. V.; Dunbrack, R. L. A Smoothed Backbone-Dependent Rotamer Library for Proteins Derived from Adaptive Kernel Density Estimates and Regressions. *Structure* **2011**, *19* (6), 844–858. https://doi.org/10.1016/j.str.2011.03.019.
(58) Li, H.; Robertson, A. D.; Jensen, J. H. Very Fast Empirical Prediction and Rationalization of Protein pKa Values. *Proteins Struct. Funct. Bioinforma.* **2005**, *61* (4), 704–721. https://doi.org/10.1002/prot.20660.
(59) Bas, D. C.; Rogers, D. M.; Jensen, J. H. Very Fast Prediction and Rationalization of pKa Values for Protein-Ligand Complexes. *Proteins Struct. Funct. Bioinforma.* **2008**, *73* (3), 765–783. https://doi.org/10.1002/prot.22102.
(60) Olsson, M. H. M.; Søndergaard, C. R.; Rostkowski, M.; Jensen, J. H. PROPKA3: Consistent Treatment of Internal and Surface Residues in Empirical p K_a Predictions. *J. Chem. Theory Comput.* **2011**, *7* (2), 525–537. https://doi.org/10.1021/ct100578z.
(61) Unni, S.; Huang, Y.; Hanson, R. M.; Tobias, M.; Krishnan, S.; Li, W. W.; Nielsen, J. E.; Baker, N. A. Web Servers and Services for Electrostatics Calculations with APBS and PDB2PQR. *J. Comput. Chem.* **2011**, *32* (7), 1488–1491. https://doi.org/10.1002/jcc.21720.
(62) Dolinsky, T. J.; Nielsen, J. E.; McCammon, J. A.; Baker, N. A. PDB2PQR: An Automated Pipeline for the Setup of Poisson-Boltzmann Electrostatics Calculations. *Nucleic Acids Res.* **2004**, *32* (Web Server), W665–W667. https://doi.org/10.1093/nar/gkh381.
(63) Kokh, D. B.; Doser, B.; Richter, S.; Ormersbach, F.; Cheng, X.; Wade, R. C. A Workflow for Exploring Ligand Dissociation from a Macromolecule: Efficient Random Acceleration Molecular Dynamics Simulation and Interaction Fingerprint Analysis of Ligand Trajectories. *J. Chem. Phys.* **2020**, *153* (12), 125102. https://doi.org/10.1063/5.0019088.
(64) Ponder, J. W.; Case, D. A. Force Fields for Protein Simulations. In *Advances in Protein Chemistry*; Elsevier, 2003; Vol. 66, pp 27–85. https://doi.org/10.1016/S0065-3233(03)66002-X.
(65) Teixeira, V. H.; Baptista, A. M.; Soares, C. M. Pathways of H2 toward the Active Site of [NiFe]-Hydrogenase. *Biophys. J.* **2006**, *91* (6), 2035–2045. https://doi.org/10.1529/biophysj.106.084376.
(66) Wang, S.; Hou, K.; Heinz, H. Accurate and Compatible Force Fields for Molecular Oxygen, Nitrogen, and Hydrogen to Simulate Gases, Electrolytes, and Heterogeneous Interfaces. *J. Chem. Theory Comput.* **2021**, *17* (8), 5198–5213. https://doi.org/10.1021/acs.jctc.0c01132.
(67) Straub, J. E.; Karplus, M. Molecular Dynamics Study of the Photodissociation of Carbon Monoxide from Myoglobin: Ligand Dynamics in the First 10 Ps. *Chem. Phys.* **1991**, *158* (2–3), 221–248. https://doi.org/10.1016/0301-0104(91)87068-7.
(68) Frisch, M. J.; Trucks, G. W.; Schlegel, H. B.; Scuseria, G. E.; Robb, M. A.; Cheeseman, J. R.; Scalmani, G.; Barone, V.; Petersson, G. A.; Nakatsuji, H.; Li, X.; Caricato, M.; Marenich, A. V.; Bloino, J.; Janesko, B. G.; Gomperts, R.; Mennucci, B.; Hratchian, H. P.; Ortiz, J. V.; Izmaylov, A. F.; Sonnenberg, J. L.; Williams; Ding, F.; Lipparini, F.; Egidi, F.; Goings, J.; Peng, B.; Petrone, A.; Henderson, T.; Ranasinghe, D.; Zakrzewski, V. G.; Gao, J.; Rega, N.; Zheng, G.; Liang, W.; Hada, M.; Ehara, M.; Toyota, K.; Fukuda, R.; Hasegawa, J.; Ishida, M.; Nakajima, T.; Honda, Y.; Kitao, O.; Nakai, H.; Vreven, T.; Throssell, K.; Montgomery Jr., J. A.; Peralta, J. E.; Ogliaro, F.; Bearpark, M. J.; Heyd, J. J.; Brothers, E. N.; Kudin, K. N.; Staroverov, V. N.; Keith, T. A.; Kobayashi, R.; Normand, J.; Raghavachari, K.; Rendell, A. P.; Burant, J. C.; Iyengar, S. S.; Tomasi, J.; Cossi, M.; Millam, J. M.; Klene, M.; Adamo, C.; Cammi, R.; Ochterski, J. W.; Martin, R. L.; Morokuma, K.; Farkas, O.; Foresman, J. B.; Fox, D. J. Gaussian 16 Rev. C.01, 2016.
(69) Mark, P.; Nilsson, L. Structure and Dynamics of the TIP3P, SPC, and SPC/E Water Models at 298 K. *J. Phys. Chem. A* **2001**, *105* (43), 9954–9960. https://doi.org/10.1021/jp003020w.
(70) Berendsen, H. J. C.; Postma, J. P. M.; Van Gunsteren, W. F.; DiNola, A.; Haak, J. R. Molecular Dynamics with Coupling to an External Bath. *J. Chem. Phys.* **1984**, *81* (8), 3684–3690. https://doi.org/10.1063/1.448118.

(71) Nosé, S. A Molecular Dynamics Method for Simulations in the Canonical Ensemble. *Mol. Phys.* **1984**, *52* (2), 255–268. https://doi.org/10.1080/00268978400101201.
(72) Hoover, W. G. Canonical Dynamics: Equilibrium Phase-Space Distributions. *Phys. Rev. A* **1985**, *31* (3), 1695–1697. https://doi.org/10.1103/PhysRevA.31.1695.
(73) Parrinello, M.; Rahman, A. Polymorphic Transitions in Single Crystals: A New Molecular Dynamics Method. *J. Appl. Phys.* **1981**, *52* (12), 7182–7190. https://doi.org/10.1063/1.328693.
(74) Nosé, S.; Klein, M. L. Constant Pressure Molecular Dynamics for Molecular Systems. *Mol. Phys.* **1983**, *50* (5), 1055–1076. https://doi.org/10.1080/00268978300102851.
(75) Hess, B.; Bekker, H.; Berendsen, H. J. C.; Fraaije, J. G. E. M. LINCS: A Linear Constraint Solver for Molecular Simulations. *J. Comput. Chem.* **1997**, *18* (12), 1463–1472. https://doi.org/10.1002/(SICI)1096-987X(199709)18:12<1463::AID-JCC4>3.0.CO;2-H.
(76) Yakovlev, D.; Boek, E. S. Structure of Bilayer Membranes of Gemini Surfactants with Rigid and Flexible Spacers from MD Simulations. In *Computational Science — ICCS 2003*; Sloot, P. M. A., Abramson, D., Bogdanov, A. V., Gorbachev, Y. E., Dongarra, J. J., Zomaya, A. Y., Eds.; Goos, G., Hartmanis, J., Van Leeuwen, J., Series Eds.; Lecture Notes in Computer Science; Springer Berlin Heidelberg: Berlin, Heidelberg, 2003; Vol. 2658, pp 668–677. https://doi.org/10.1007/3-540-44862-4_72.
(77) Darden, T.; York, D.; Pedersen, L. Particle Mesh Ewald: An $N \cdot \log(N)$ Method for Ewald Sums in Large Systems. *J. Chem. Phys.* **1993**, *98* (12), 10089–10092. https://doi.org/10.1063/1.464397.
(78) Cheatham, T. E. I.; Miller, J. L.; Fox, T.; Darden, T. A.; Kollman, P. A. Molecular Dynamics Simulations on Solvated Biomolecular Systems: The Particle Mesh Ewald Method Leads to Stable Trajectories of DNA, RNA, and Proteins. *J. Am. Chem. Soc.* **1995**, *117* (14), 4193–4194. https://doi.org/10.1021/ja00119a045.
(79) Chovancova, E.; Pavelka, A.; Benes, P.; Strnad, O.; Brezovsky, J.; Kozlikova, B.; Gora, A.; Sustr, V.; Klvana, M.; Medek, P.; Biedermannova, L.; Sochor, J.; Damborsky, J. CAVER 3.0: A Tool for the Analysis of Transport Pathways in Dynamic Protein Structures. *PLoS Comput. Biol.* **2012**, *8* (10), e1002708. https://doi.org/10.1371/journal.pcbi.1002708.
(80) Magdziarz, T.; Mitusińska, K.; Bzówka, M.; Raczyńska, A.; Stańczak, A.; Banas, M.; Bagrowska, W.; Góra, A. AQUA-DUCT 1.0: Structural and Functional Analysis of Macromolecules from an Intramolecular Voids Perspective. *Bioinformatics* **2020**, *36* (8), 2599–2601. https://doi.org/10.1093/bioinformatics/btz946.
(81) Schrödinger, LLC. The PyMOL Molecular Graphics System, Version 1.8, 2015.

For Table of Contents Only